Front. Optoelectron. 2017, 10(1): 80–88
DOI 10.1007/s12200-017-0665-0

RESEARCH ARTICLE

# Reducing the negative effects of flywheel disturbance on space camera image quality using the vibration isolation method

**Changcheng DENG (✉)[1,2], Deqiang MU[3], Junli GUO[1], Peng XIE[1]**

1 Institute of Optics, Fine Mechanics and Physics, Chinese Academy of Sciences, Changchun 130033, China
2 University of Chinese Academy of Sciences, Beijing 100039, China
3 Changchun University of Technology, Changchun 130012, China



**Abstract** Although the performance of space cameras has largely improved, the micro vibration from flywheel disturbances still significantly affects the image quality of these cameras. This study adopted a passive isolation method to reduce the negative effect of flywheel disturbance on image quality. A metal-rubber shock absorber was designed and installed in a real satellite. A finite element model of an entire satellite was constructed, and a transient analysis was conducted afterward. The change in the modulate transfer function was detected using ray tracing and optical transfer function formulas. Experiments based on real products were performed to validate the influence of the metal-rubber shock absorber. The experimental results confirmed the simulation results by showing that the negative effects of flywheel disturbance on the image quality of space cameras can be diminished significantly using the vibration isolation method.

**Keywords** micro vibration, modulate transfer function, vibration isolation, flywheel disturbance

## 1 Introduction

Space cameras are useful in studying the surface of the earth for their ability to obtain objective information that can be widely used in several domains, including topographic maps, geological survey, forest resources survey, urban design and renovation, railways, highways, and other transit exploration. The influence of micro vibration on image quality has become increasingly significant along with the continuous improvement of space cameras.

Satellites need movable parts to function, including attitude-controlling reaction flywheels, control moment gyroscopes, reaction jet devices, energy-providing solar panels, and other agencies. The movement of these parts generates various degrees of micro vibration [1]. Despite not damaging the satellite structure, such micro vibration affects the pointing accuracy and stability of a space optical remote sensing satellite, obstructs the transfer of the photo-inducing charge and the motion synchronization of the focal plane image, and affects the quality of camera images [2]. These effects restrict the developments in space optical remote sensing technology. Given that flywheel disturbance is the main source of micro vibration [3], eliminating the effects of the flywheel rotary actuator disturbance on space cameras has become a key technology of high-precision stabilized platforms for spacecraft.

The flywheel disturbance results from the imbalance of the flywheel rotor, which in turn can be attributed to the following factors:

1) uneven material quality, poor manufacturing precision, and structural asymmetry during fabrication,

2) poor installation, eccentricity, and loose parts during assembly and installation, and

3) shaft bending and deformation as well as wear, corrosion, fracture, or deposition of the rotating parts during the operation of the satellite [4,5].

Micro vibration changes the relative position of the optical element, the alignment of optical components, and the line of sight of the camera. In this case, micro vibration can change the imaging position, system aberration, and image quality. Micro vibration is a dynamic process, and the relative position of optical components changes with time. Therefore, the effect of micro vibration on the image

Received August 29, 2016; accepted December 12, 2016

E-mail: changcheng0211@163.com

quality of optical components also changes along with time [6].

By changing the surface shapes of the optical element, micro vibration directly affects image quality. The effects of micro vibration on the changes in surface shape also vary along with time. Previous studies show that the effects of the changes in surface shape on image quality are much smaller than the negligible effects of line of sight [7].

Provided an ideal optical system for imaging an object point, it should be formed a point. If micro vibration is generated during the imaging process, then the point in the imaging position will be changed. According to geometrical optics, the point will be imaged at several locations, thereby decreasing the light intensity, expanding the range of light distribution, lowering the image contrast, and reducing the resolution.

Flywheel disturbance has a relatively wide bandwidth, while the altitude control system has a generally small bandwidth. Therefore, flywheel disturbance cannot be easily measured and controlled. This study refers to the results of a computer simulation analysis. Only few studies have conducted a micro vibration test using an optical space camera with a long focal length. This paper investigated the influence of flywheel disturbance on the image quality of a camera by conducting a simulation and an experiment. A passive isolation method was adopted to reduce the micro vibration generated by the flywheel disturbance. A metal-rubber shock absorber was designed and installed in a real satellite. The main innovation of this paper lies in the fact that we have conducted an experiment based on real products to test the modulate transfer function (MTF) even if experiments of such nature are often difficult to realize.

## 2 Design of the metal-rubber shock absorber

Many isolation devices have been designed for different rockets, of which the Stewart platform is the most popular. This platform was introduced by the American scholar Stewart in 1965 [8] when he designed a flight simulator with six degrees of freedom. This platform is known for its simple design, large carrying capacity, high precision, and minimal components. However, if one actuator malfunctions, then the results will be catastrophic. This platform also requires specific assembling for decoupling control, and the centroid of load must be placed at the center of the platform. These requirements are difficult to achieve, especially for aerospace application.

A system with eight damping pads (metal-rubber shock absorbers) was designed based on the Stewart platform. These pads were uniformly distributed in a circle as shown in Fig. 1, and the system was mounted on the isolation structure. Apart from having two additional damping elements, this design has a higher reliability and carrying capacity than the original Stewart platform. Most importantly, this design only requires the centroid of load to be placed on the main axis of the platform.

Figure 2 presents the structure of a metal-rubber shock absorber [9–11], which comprises upper and lower parts with parallel stiffness. The axis load during flight is only applied on the lower part. The metal-rubber shock absorber has spring and damping features and can constrain the translation of the equipment by mounting the structure in three directions. The entire mounting structure of the camera is suspended on the platform of eight damping pads, and the vibration is reduced in three directions.

The thickness, area, and distribution diameter of the absorbers must be carefully selected to create an excellent dynamic environment and meet the requirement of roll stiffness.

The metal-rubber shock absorber comprises a metal wire with a 0.15 mm diameter. The wire is evaluated according to the structure of the absorber and by several circles of optimal design and experiment. The metal-rubber shock absorber has a diameter of $\varphi$ = 50 mm, and its upper and lower parts have thicknesses of 25 and 15 mm,

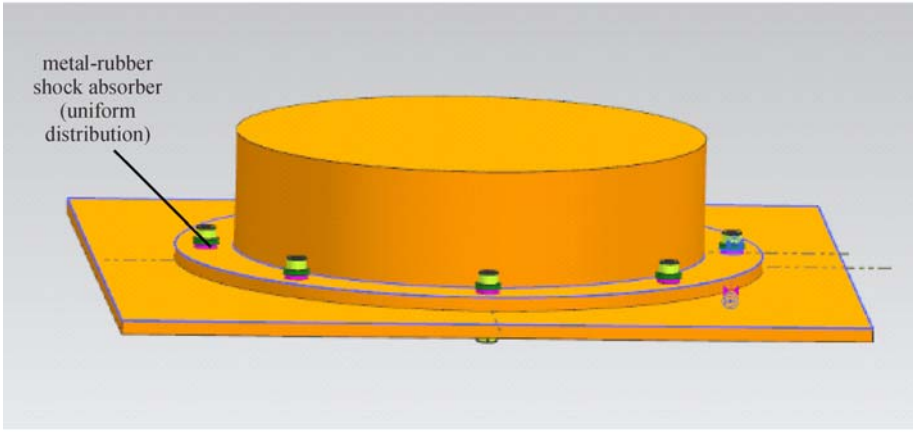


**Fig. 1** Metal-rubber shock absorber with eight damping pads

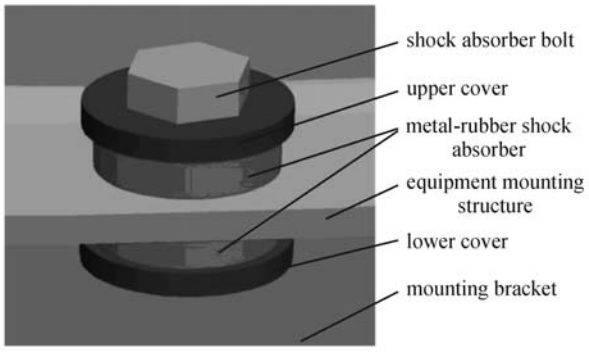


**Fig. 2** Structure of a damping pad

respectively. The absorber has a total density of 1.4 g/cm$^3$ and is compressed by 30% of its original size, which means that the damping ratio ranges between 0.06 and 0.1.

## 3 Finite element modeling and results

Three flywheels were included in the finite element model and mounted on the main back plate. Figure 3 presents the positions of these flywheels.

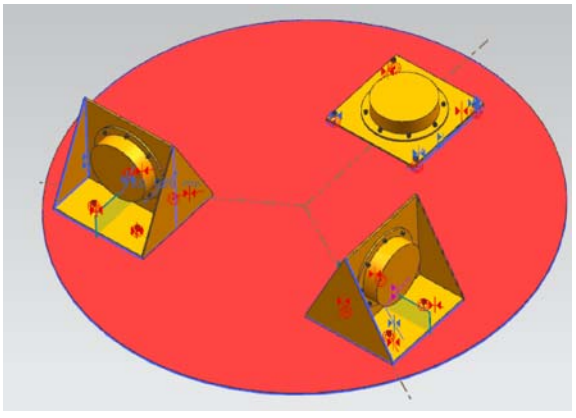

**Fig. 3** Positions of flywheels

The finite element model of the entire satellite was constructed using the Patran/Nastran MSC software as shown in Fig. 4. The entire satellite model, which comprised 33893 nodes and 21856 elements, was used to obtain the displacements of all lenses. The model had no displacement constraints.

The forces and moments model of the flywheel was generated in the experiments. Figure 5(a) presents the test platform, and Fig. 5(b) presents an example of $F_y$. The tested forces and moments on the location of the flywheel were added in the finite element model.

Table 1 lists the loading conditions that are investigated in this study.

Figure 6 presents the arrangement of the mirrors, while

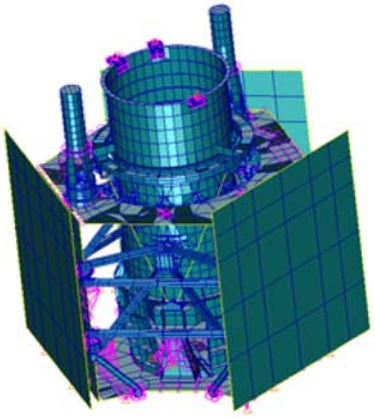

**Fig. 4** Finite element model of the entire satellite

Figs. 7 and 8 show the displacements of all lenses as obtained via transient analysis. Unlike case 3, case 2 had no vibration isolation. The displacements greatly differed upon the addition of vibration isolation. Table 2 lists the meanings of the related nodes. The displacements of the primary, second, third, folding, and focusing mirrors as well as those of the image plane in the $y$, $z$ direction ($x$-axis is the optical axis in the finite model) were imported from Patran into Matlab, and then each set of vibration data was sent to ZEMAX via a dynamic link. The vibration information of the displacements of a light spot in the image plane at the sampling time was obtained via ray tracing.

Ray tracing [12] calculates the direction and position of the outgoing ray based on the incident ray, reflection law, and structural parameters, including the radius, thickness, and refractive index of the lens. The right-handed coordination system was used in the analysis to determine the symbol of angles and lines. The optical axis coincided with the $z$-axis, and the coordinate originated from the sphere vertex. The state of the incident light was represented by the position vector of light $T$ and the unit vector of the direction of light propagation $Q^0$. The state of the incident ray can be expressed as follows:

$$\begin{cases} T(x,y,z) = xi + yj + zk, \\ Q^0(\alpha,\beta,\gamma) = \alpha i + \beta j + \gamma k, \end{cases} \tag{1}$$

where $i$, $j$, and $k$ are the unit vectors along the $x$-, $y$-, and $z$-axes, respectively. Given that they are unit vectors, $\alpha$, $\beta$, $\gamma$ are three directional cosines. The state of the refractive ray $T_1$, $Q_1^0$ can be expressed as follows:

$$\begin{cases} T_1(x,y,z) = x_1 i + y_1 j + z_1 k, \\ Q_1^0(\alpha,\beta,\gamma) = \alpha_1 i + \beta_1 j + \gamma_1 k. \end{cases} \tag{2}$$

Provided that the radius of the curvature of the refractive surface is $r$, the refractive indexes are $n$ and $n'$, and the interval distance between the two spheres of the lens is

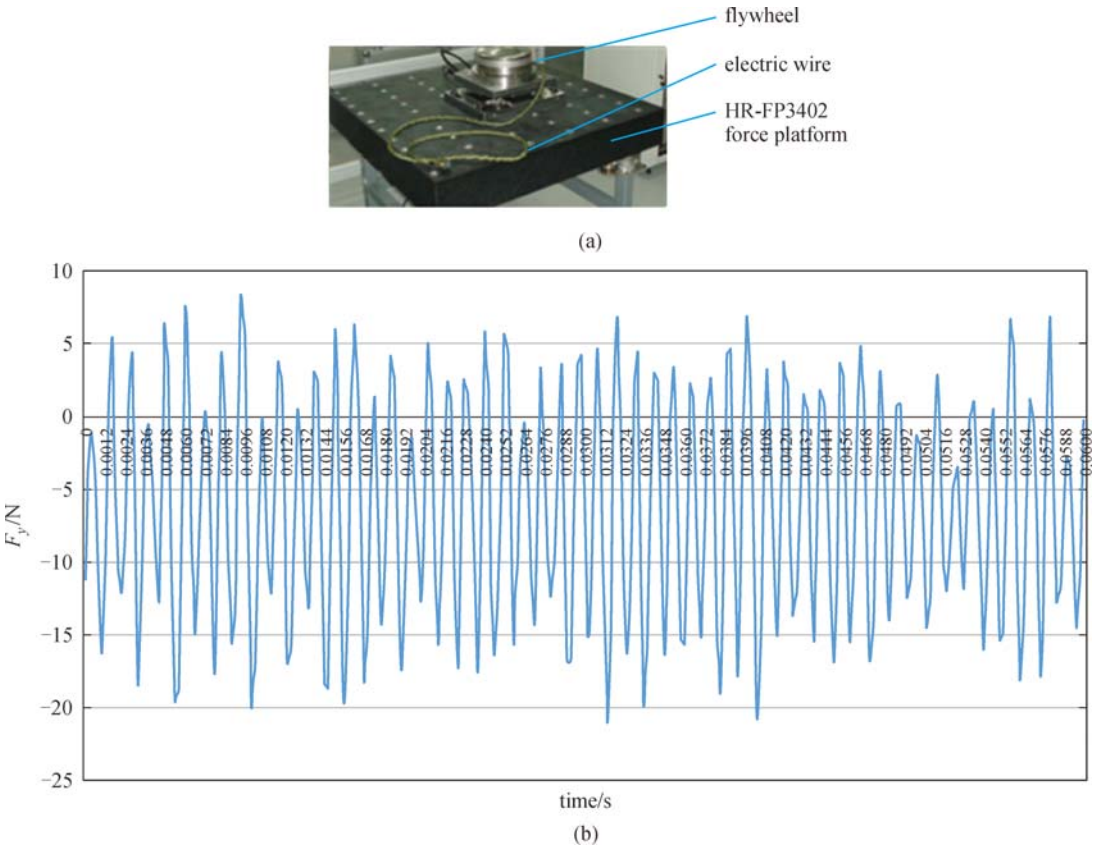


**Fig. 5** Test platform (a) and tested force result (b) of the flywheel

**Table 1** Loading conditions in the flywheel disturbance experiment

| cases | flywheel rotation | vibration isolation |
|---|---|---|
| 1 | without | without |
| 2 | with | without |
| 3 | with | with |

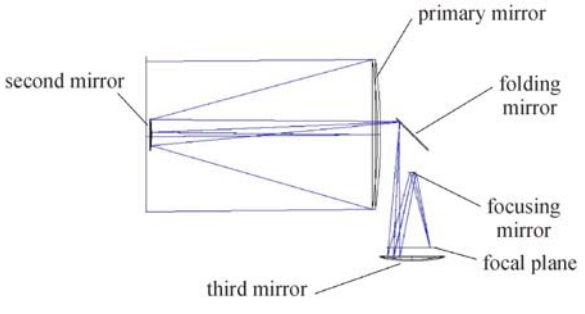


**Fig. 6** Arrangement of the six mirrors

known, the refractive light can be calculated by coordinating the incident light.

All light spot image displacements in the exposure at the image plane can be obtained by repeating each sampling data in integration time. The displacement can be interpreted as the distribution of the image shift probability of the sample that is induced by vibration. The optical transfer function (OTF, Eq. (3)) and $N$-order statistical moments (Eq. (4)) were used to calculate the imaging MTF of the vibration [13]. Figure 9 presents the flowchart.

$$\mathrm{OTF}(\omega) = \sum_{n=0}^{\infty} \frac{m_n}{n!}(-\mathrm{j}\omega)^n, \tag{3}$$

$$m_n^x = \frac{1}{S}\sum_{i=1}^{s} x_i^n, \tag{4}$$

where OTF is the optical transfer function, $\{x_i\}(i = 1,2,3,...,S)$ is the sampling sequence, and $m_n^x$ is the $N$-order statistical moments of movement.

Figure 10 presents the coordinates of spot displacement in the focal plane. The displacement curves were random and did not follow a regular pattern. The displacement was used as the basis for calculating MTF. Figure 11 shows the MTF at Nyquist frequency (57 lp/mm, which reflects the system performance) for the three cases listed in Table 1. Case 1 had an MTF of 0.124 along the $x$- and $y$-axes because these axes were identical. Case 2 had MTFs of 0.105 along the $x$-axis (the $z$-axis is the optical axis in the optical system) and 0.085 along the $y$-axis, thereby

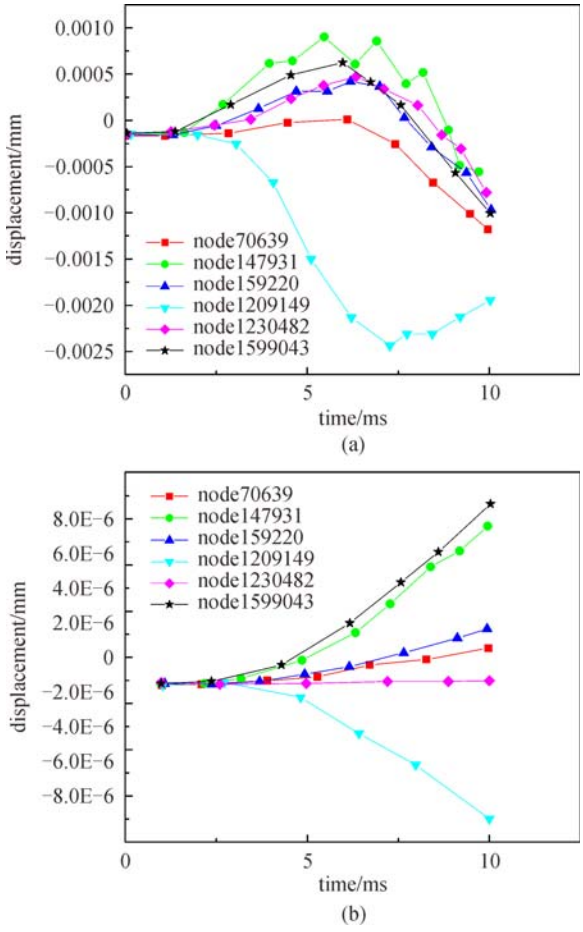


**Fig. 7** Displacements in the *y*-axis without (a) and with (b) the metal-rubber shock absorber

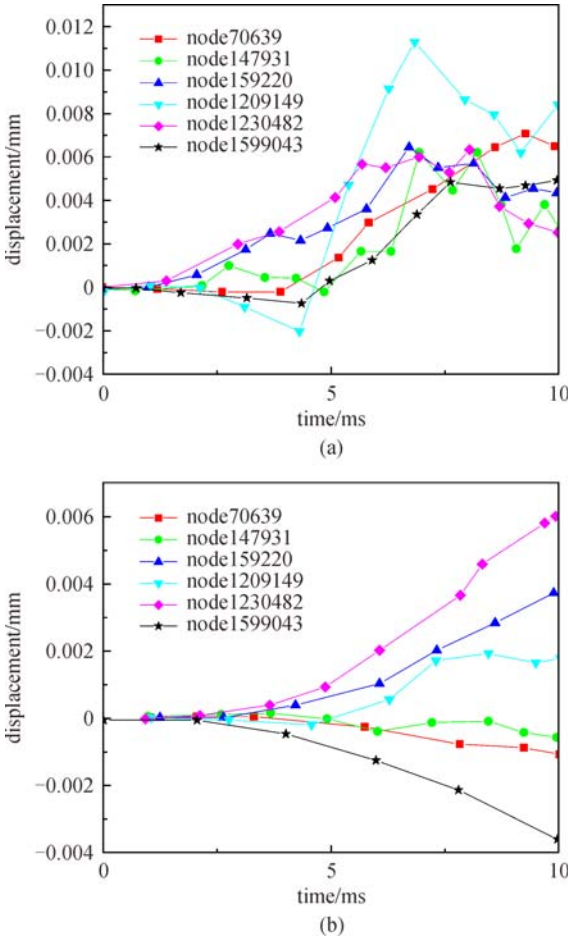


**Fig. 8** Displacement in the *z*-axis without (a) and with (b) the metal-rubber shock absorber

achieving an average MTF of 0.095. Case 3 had MTFs of 0.118 along the *x*-axis and 0.112 along the *y*-axis, thereby achieving an average MTF of 0.115. The MTF decreased by 23% from cases 1 to 2, but increased by 21% from cases 2 to 3.

## 4 Experiments and results

### 4.1 Experimental setup

The experimental equipment included a satellite, camera, metal-rubber shock absorbers, three reaction flywheels, collimator, air flotation platform, CCD components, knife edge target, alignment equipment, data acquisition system, and computer. The *z*-axis was the optic axis, while the other axes were dependent by right hand.

The experiment test objects included an optical camera, a satellite platform, and a flywheel, all of which were mounted on an air flotation platform as shown in Fig. 12. The static target was illuminated by the light source, and the light passed through the collimator and lenses of the camera. The light focused on the focal plane, and the CCD sensor was used to capture images. The image of the knife edge target was generated by the system. The data were acquired using the ground image acquisition and processing system, and the corresponding MTF was calculated using the knife edge method.

**Table 2** Meanings of nodes

| node | mirror |
|---|---|
| 70639 | primary mirror |
| 147931 | focal plane |
| 159220 | folding mirror |
| 1209149 | second mirror |
| 1230482 | focusing mirror |
| 1599043 | third mirror |

### 4.2 Knife edge method

Figure 13 presents the flowchart of the knife edge image analysis method, which follows three basic steps [14,15].

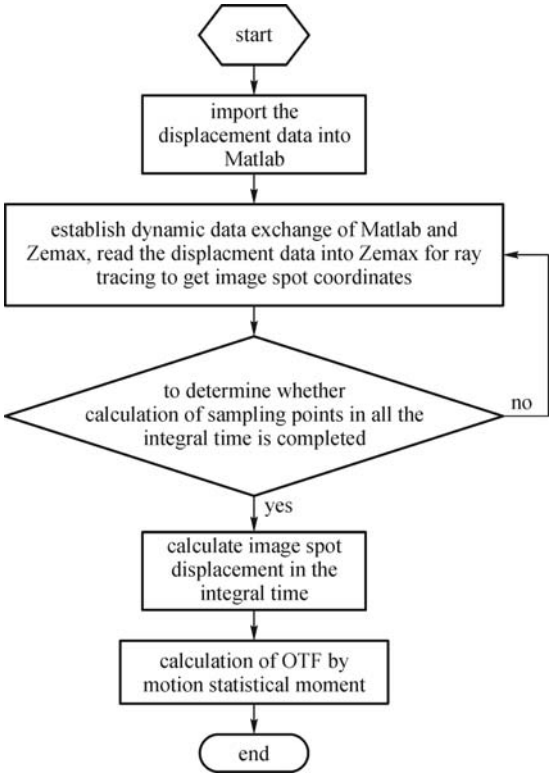


**Fig. 9** MTF calculation flowchart

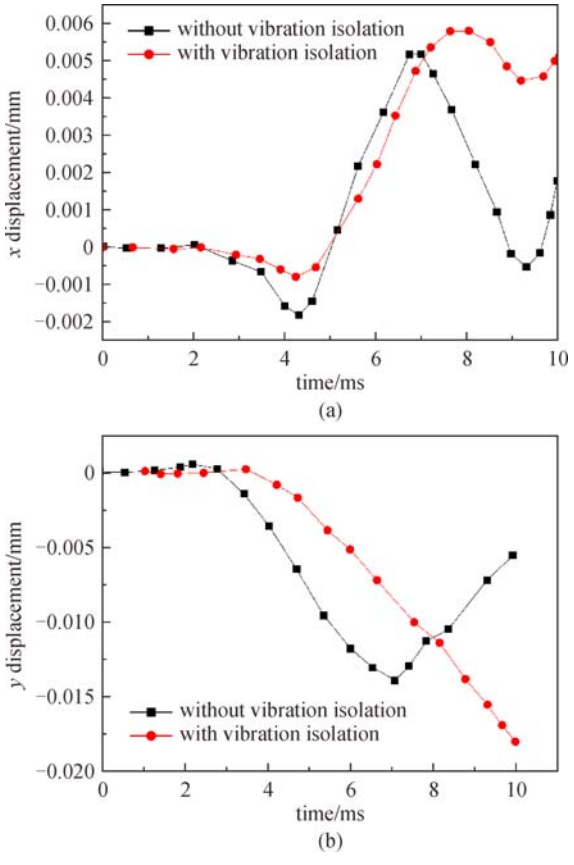


**Fig. 10** Spot displacements in the focal plane along the *x*- (a) and *y*-axes (b)

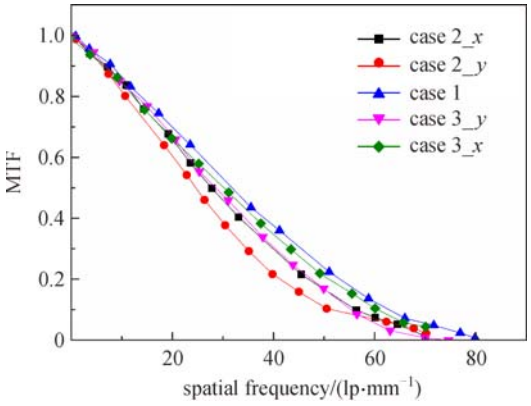


**Fig. 11** Effect of vibration on MTF

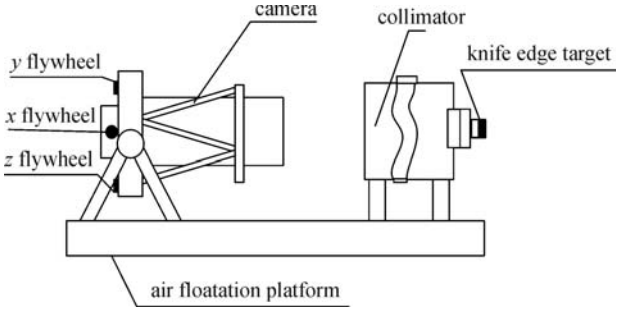


**Fig. 12** Schematic of the satellite test setup

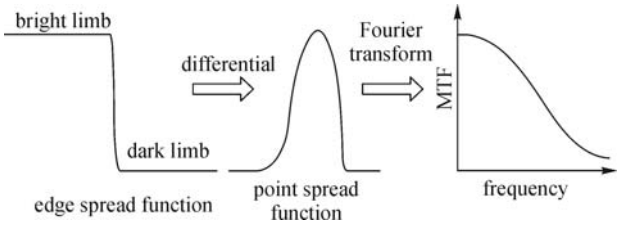


**Fig. 13** Steps of the knife edge image analysis method

First, remove the noises from the test system and fit image, and then obtain the edge spread function. Second, obtain the point spread function using the differential of the edge spread function. Third, obtain the MTF using the Fourier transform of the point spread function.

### 4.3 Experimental results and analysis

The transfer function of the camera was tested in the three cases listed in Table 1. Figures 14 to 16 show the real-time transfer function curves of these cases.

Case 1 had a mean MTF of 0.119, which decreased by 21% to 0.094 in case 2 because of flywheel rotation and increased to 0.114 in case 3 after the addition of the absorber. The micro vibration of the flywheel rotation reduced the image quality of the camera, and such

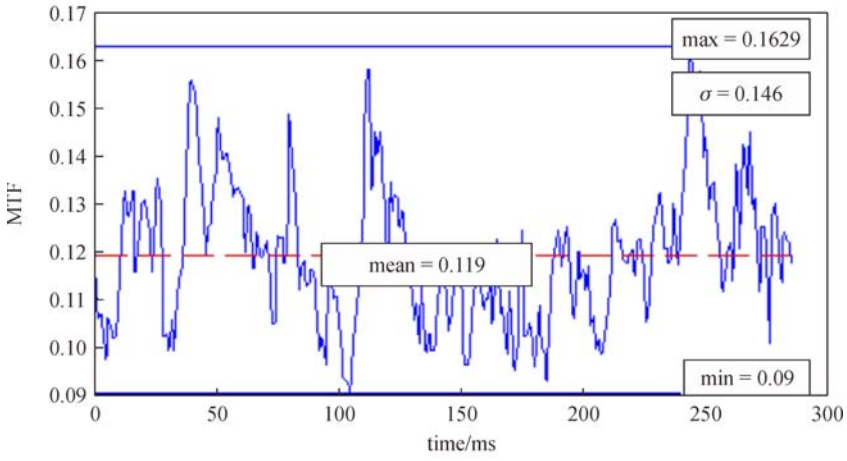


**Fig. 14** MTF without flywheel disturbance and vibration isolation

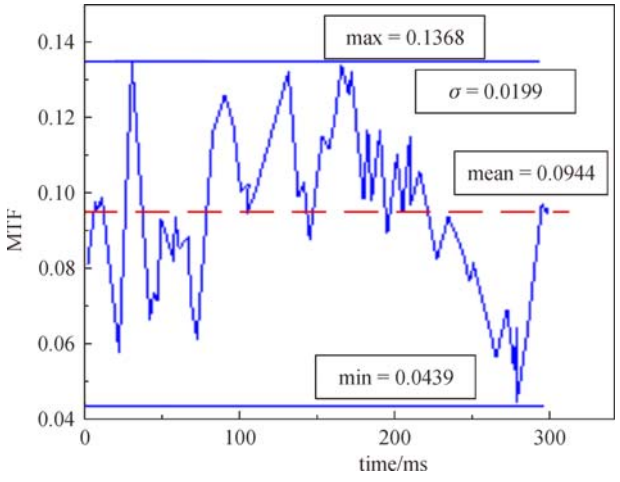


**Fig. 15** MTF with flywheel disturbance and without vibration isolation

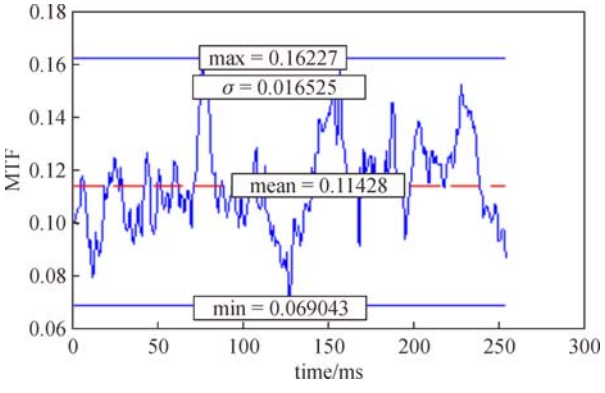


**Fig. 16** MTF with flywheel disturbance and vibration isolation

reduction can be diminished effectively using the vibration isolation method.

The experimental results matched the simulation results even though the MTF in the simulation was slightly larger than that in the experiments. Such difference could be explained by the low sensitivity of the finite element to the variations in displacement. The stiffness of the whole satellite increased in the simulation if the fit nodes outnumber the contact nodes at bolt. The experiment had a monochromatic aberration, chromatic aberration, image algorithm error, and principle for assessing image quality and noise impact, all of which can lead to a low MTF.

## 5 Discussion

The vibration can be controlled using several methods, including electronic image stabilization, optical image stabilization, passive vibration isolation, semi-active vibration isolation, and active vibration isolation [16]. To fulfill the requirement of high reliability in aerospace

application, the passive isolation method is often used as this technique does not require an external energy input, maintains the stability of the system, and evidently shows the isolation effect on high-frequency vibration.

The movement of the reaction flywheel can generate high-frequency sinusoidal vibration. The vibration isolation mechanism is equivalent to a high-frequency sinusoidal vibration being applied to a low-pass filter; therefore, the reaction flywheel acting on the satellite mainly generates low-frequency sinusoidal vibration.

In a passive vibration isolation scheme, the requirements for the safe operation of the carrier and aircraft can be fulfilled by selecting reasonable parameters, including the diameter, thickness, and distributed diameter of the vibration isolation. To reduce the negative effects of micro vibration, the following factors must be considered:

1) disturbance characteristics of the micro vibration source (reaction flywheel);

2) satellite structure and vibration isolation requirements of on-board equipment; and

3) imaging conditions of the camera in orbit and the integral series of charge coupled device time delay integration.

## 6 Conclusion

The micro vibration from the flywheel affects the image quality of space cameras. A passive isolation method is applied to reduce the effect of micro vibration and improve the image quality of space cameras. A metal-rubber shock absorber is designed and installed in a real satellite.

A finite element model of an entire satellite is constructed, and an experimental system is designed based on a real satellite. The MTF of the system is used as a criterion of image quality. Three loading cases are investigated, including cases without disturbance and vibration isolation, with disturbance and without vibration isolation, and with disturbance and vibration isolation. The simulation and experimental results showed that the vibration of the flywheel reduced the image quality of the camera by almost 20%, and this effect was diminished upon the addition of the metal-rubber shock absorber.

**Acknowledgements** The author thanks the Changchun Institute of Optics, Fine Mechanics and Physics, Chinese Academy of Sciences for their assistance in the experiment. This work was supported by the National High Technology Research and Development Program of China (863 Program) (No. 2012AA121502).

## References

1. Pang S, Yang L, Qu G. New development of micro-vibration integrated modeling and assessment technology for high performance spacecraft. Structure & Environment Engineering, 2007, 34 (6): 1–9
2. Zhong W C. Spacecraft obit and attitude parameters impact analysis for optical imaging. Dissertation for the Master Degree. Haerbin: Harbin Institute of Technology, 2009
3. Lee D O, Yoon J S, Han J H. Development of integrated simulation tool for jitter analysis. International Journal of Aeronautical and Space Sciences, 2012, 13(1): 64–73
4. Masterson R A, Miller D W, Grogan R L. Development and validation of reaction wheel disturbance models:empirical model. Journal of Sound and Vibration, 2002, 249(3): 575–598
5. Han X. Satellite jitter analysis based on unbalance of flywheel. Aerospace Shanghai, 2012, 29(6): 42–45
6. Zhang B, Wang X, Hu Y. Integrated analysis on effect of micro-vibration on high resolution space camera imaging. Spacecraft Recovery & Remote Sensing, 2012, 33(2): 60–66
7. Wang H, Wang W, Wang X, Zou G, Li G, Fan X. Space camera image degradation induced by satellite micro-vibration. Acta Photoning Sinica, 2013, 42(10): 1212–1217
8. Stewart D. A platform with six degree of freedom. Proceedings-Institution of Mechanical Engineers, 1965, 180(1): 371–386
9. Klenke S, Baca T. Structural dynamics test simulation and optimization for aerospace components. Expert Systems with Applications, 1996, 11(4): 82–89
10. Rudoler S, Hadar O, Fisher M, Kopeika N S. Image resolution limits resulting from mechanical vibration. Optics and Precision Engineering, 1991, 30(5): 577–589
11. Fu M, Liu Y, Cui M, Cao M. Metal-rubber vibration absorber for aerocraft. Optics and Precision Engineering, 2013, 21(5): 1174–1182
12. Wang J.Evaluation and optimization on dynamic imaging quality of an optical remote sensor. Dissertation for the Doctoral Degree. Changchun: Changchun Institute of Optics, Fine Mechanics and Physics, 2000
13. Zhang Y. Imaging MTF of space camera under vibration and simulation. Optics and Precision Engineering, 2011, 19(9): 2146–2153
14. Schowengerdt R A, Basedow R W, Colwell J E. Measurement of the HYDICE system MTF from flight imagery. SPIE Proceedings, 1996, 2821: 127–136
15. Léger D, Duffaut J, Robinet F. MTF measurement using spotlight. IEEE Proceedings of IGARRS, 1994, 4: 2010–2012
16. Liu C, Jing X, Daley S, Li F. Recent advances in micro-vibration isolation. Mechanical Systems and Signal Processing, 2015, 56–57: 55–80

**Changcheng Deng** is a Ph.D. student at Changchun Institute of Optics, Fine Mechanics and Physics, Chinese Academy of Sciences. His current research interests include the mechanical vibration of space remote sensors.
Email: changcheng0211@163.com

**Deqiang Mu** received his Ph.D. degree in 2001 from Jilin University, Changchun, China. He is currently working at the Changchun University of Technology. His current research interests include mechanical dynamics, design optimization, and measurement and control technologies for manufacturing processes.
Email: mudq@mail.ccut.edu.cn

**Junli Guo** received his master's degree in 2016 from the Changchun Institute of Optics, Fine Mechanics and Physics, Chinese Academy of Sciences. He is currently working at the Institute of Optics and Electronics. His current research interests include spatial mirror support and lightweight design.
Email: junli_guo@yeah.net

**Peng Xie** received his M.S. degree in 2010 from the Changchun Institute of Optics, Fine Mechanics and Physics, Chinese Academy of Sciences. He is currently working as a research assistant at the same institute. His research interests include the opto-mechanical system design of space cameras.
E-mail: wl2sbq1314@126.com